

Flipping chiral edge states through nuclear spin S in vdW magnets

Kaushal Kumar Kesharpu

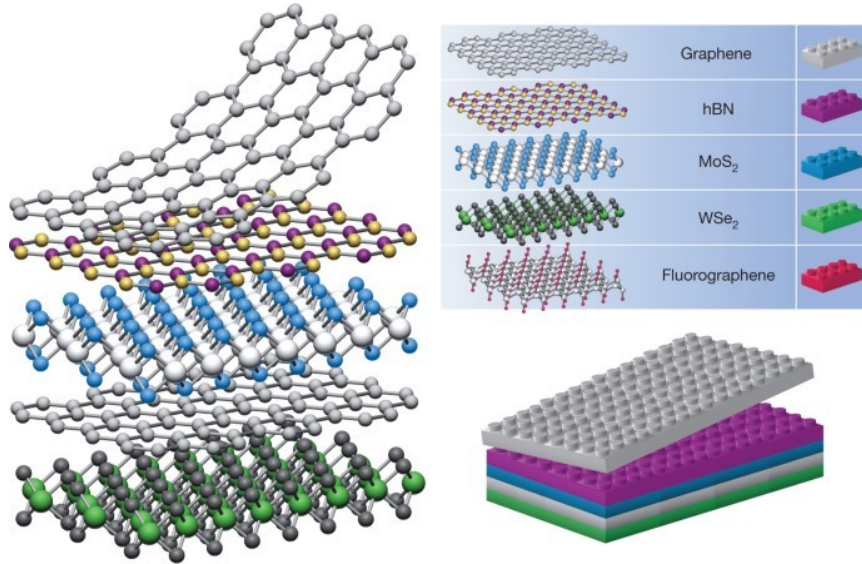
Bogoliubov Laboratory of Theoretical Physics,
Joint Institute for Nuclear Research,
Dubna, Russia

Publications

- 1) **K. K. Kesharpu**, E. A. Kochetov, and A. Ferraz, **Physical Review B** **107**, 155146 (2023).
- 2) **K. K. Kesharpu**, arXiv:2305.13423, submitted to PRB (second round review)

What are Van Der Waals (vdW) magnets and
where it can be applied?

Van Der Waals (vdW) Magnet



Most of the magnetic vdW materials are layered, cleavable **transition-metal chalcogenides and halides**, and typically have a layer of metal ions sandwiched between layers of chalcogens or halides.

Physics investigated in vdW

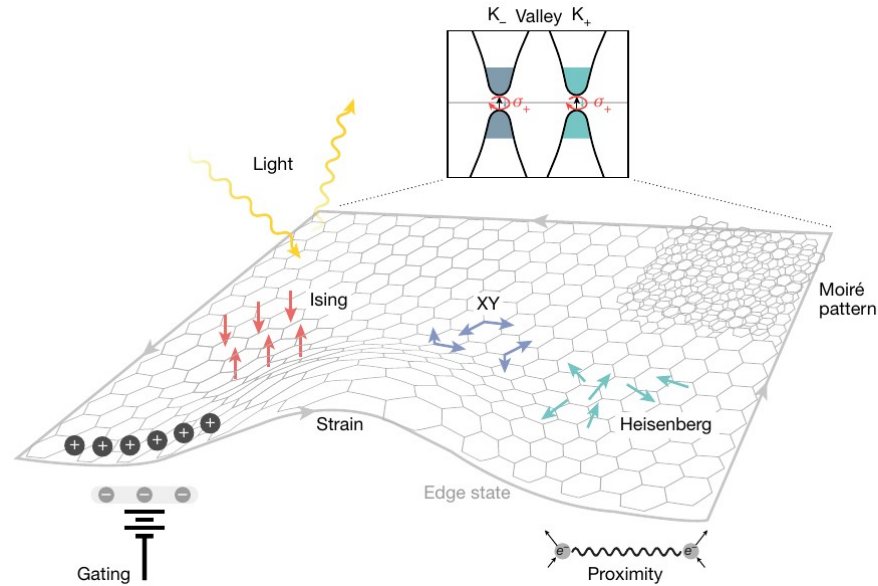
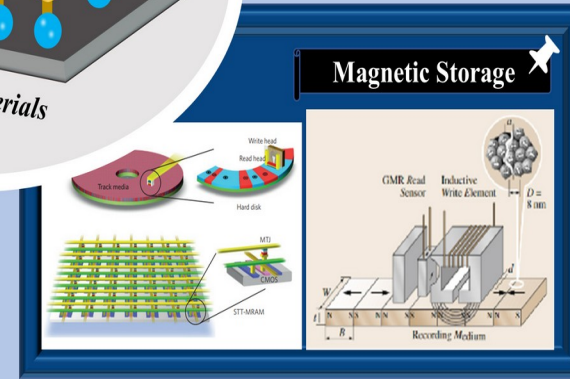
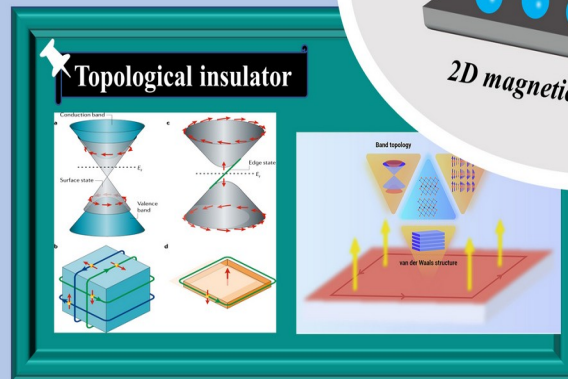
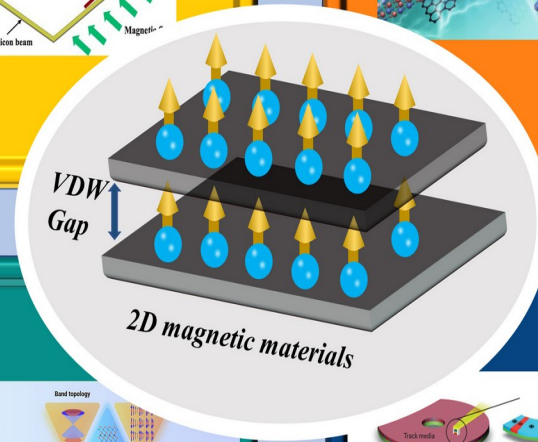
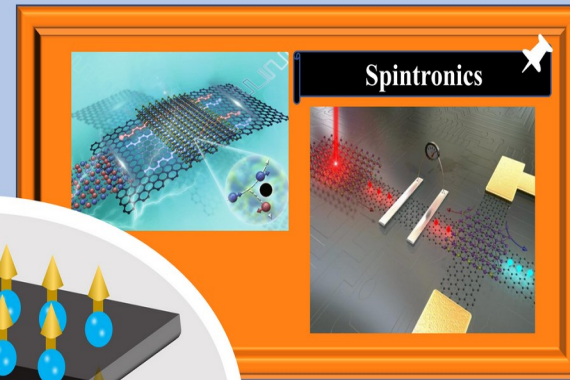
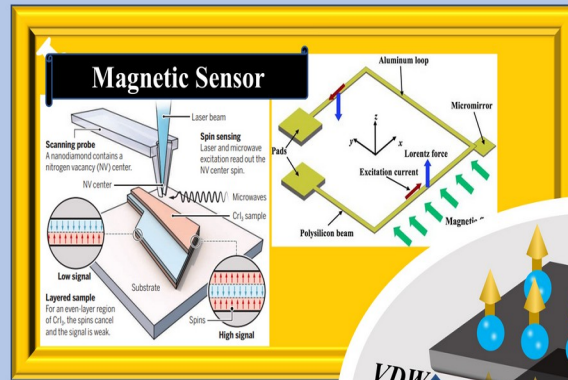


Fig. 1 | Physical phenomena that can be studied with magnetic vdW materials. 2D magnetic vdW materials are an ideal platform for investigating how the Hamiltonians of the fundamental magnetism models (the Ising, XY and Heisenberg models; magnetic moments indicated by the red, purple and cyan arrows, respectively) behave in the 2D limit. In addition, the magnetic ground states of these materials could be controlled

by external perturbations, such as gating and strain, or via proximity effects and moiré patterns. Because of the intrinsic properties of their honeycomb lattice, there is also a possibility of light-matter interactions through valley coupling of K_- and K_+ points in the momentum space and the edge states (grey arrows).

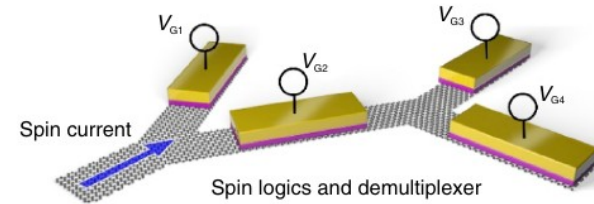
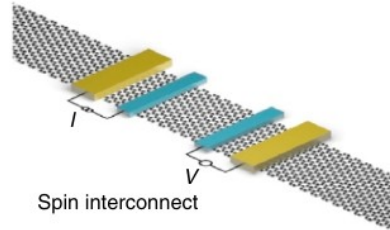
Application of vdW



Application of vdW in spintronics

Spin communication
Weak SOC

Xenes (multilayer) graphene,
black phosphorus



Spin injection and detection
2D magnets, CSI, opto-spintronics

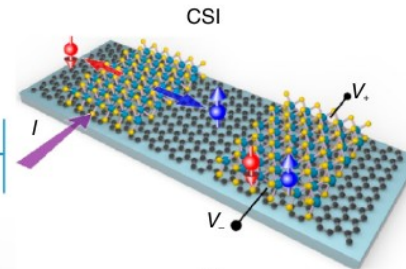
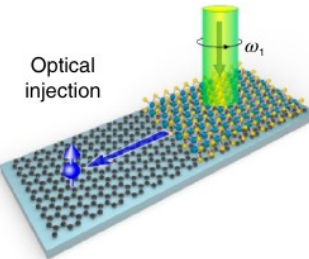
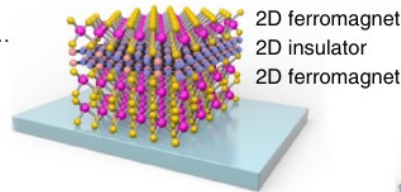
FM/AFM CrI₃, VSe₂, CrSe₂, Cr₂Ge₂Te₆, MnPSe₃...

Insulators hBN

TMDCs MoS₂, MoSe₂, WTe₂...

Topological insulators 2D: heavy xenes
3D: (Bi,Sb)₂(Te,Se)₃, α-Sn...

Magnetic tunnel junction

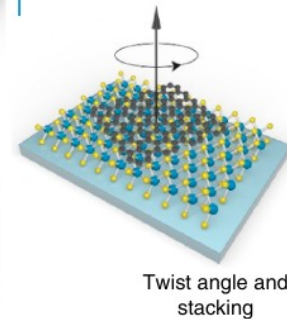
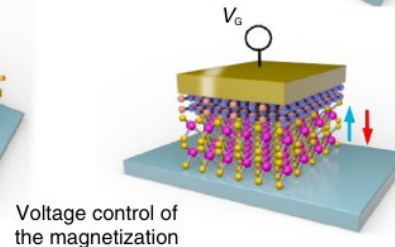
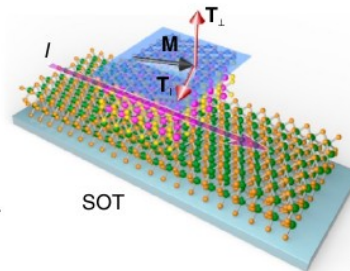


Spin manipulation and control
Strong SOC

FM/AFM CrI₃, VSe₂, CrSe₂, Cr₂Ge₂Te₆, MnPSe₃...

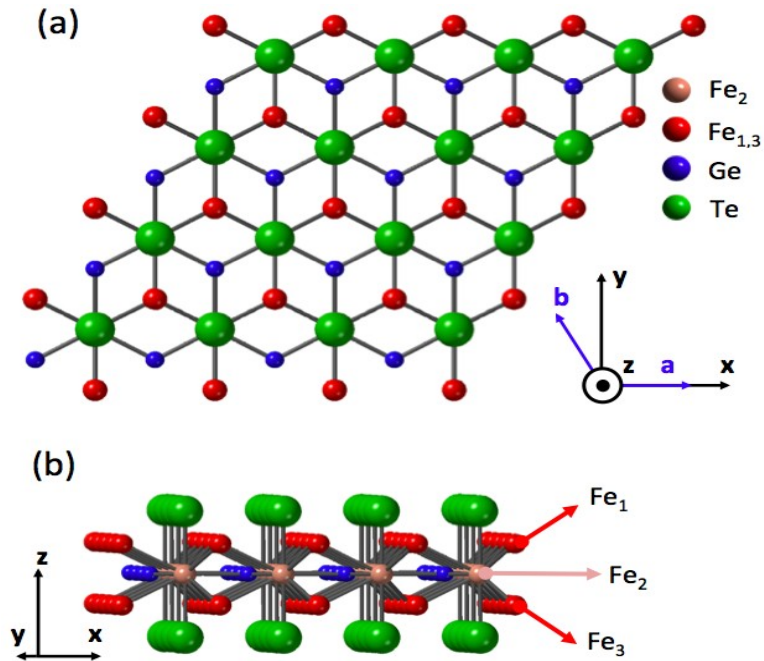
TMDCs MoS₂, MoSe₂, WTe₂...

Topological insulators 2D: heavy xenes
3D: (Bi,Sb)₂(Te,Se)₃, α-Sn...



Two important vdW magnets

Fe₃GeTe₂



Cr-X₃ (X=I, Br, Cl)

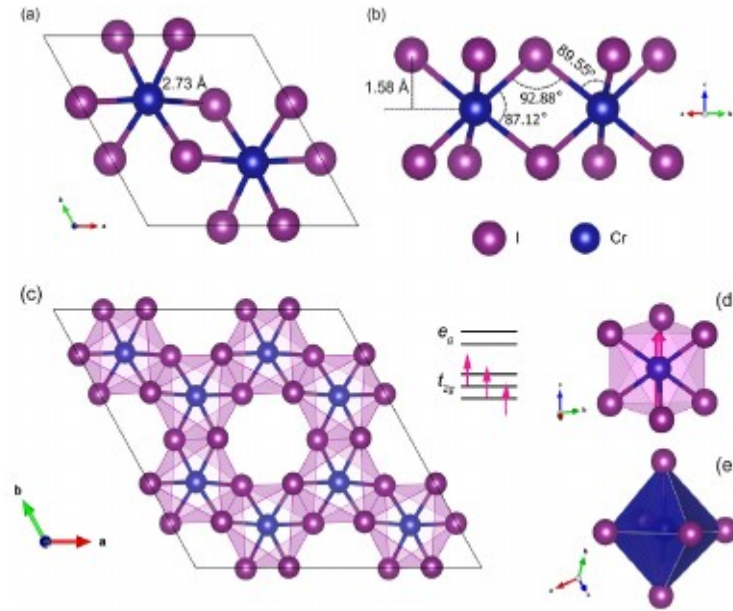


Fig. 1. Schematic illustration of the single-layer CrI₃ unit cell: bond length of Cr-I (a), bond angles and vertical distance between the plane containing I atoms and the plane containing Cr atoms (b), top view of CrI₃ crystalline structure, showing the honeycomb arrangement of the Cr atoms (c), side view of a single Cr site with an arrow representing its out-of-plane magnetic moment and the splitting of d-levels into a higher energy e_g doublet and a lower energy t_{2g} triplet in an octahedral environment (d), and the edge-sharing octahedral Cr³⁺ ion with six I⁻ ions (e).

In both Fe_3GeTe_2 and Cr-X_3 following **properties** are observed:

- 1) Strong e-e correlation**
- 2) Non-collinear spin structures on the surface**

Candidate materials CrI_3 have strong correlation

PHYSICAL REVIEW B **105**, 205124 (2022)

Dynamical correlations in single-layer CrI_3

Yaroslav O. Kvashnin,¹ Alexander N. Rudenko,^{2,*} Patrik Thunström,¹ Malte Rösner,² and Mikhail I. Katsnelson²

¹Division of Materials Theory, Department of Physics and Astronomy, Uppsala University, Box 516, SE-751 20 Uppsala, Sweden

²Institute for Molecules and Materials, Radboud University, Heyendaalseweg 135, 6525 AJ Nijmegen, The Netherlands

 (Received 19 January 2022; revised 6 April 2022; accepted 6 May 2022; published 20 May 2022)

Chromium triiodide is an intrinsically magnetic van der Waals material down to the single-layer limit. Here, we provide a first-principles description of finite-temperature magnetic and spectral properties of monolayer (ML) CrI_3 based on fully charge self-consistent density functional theory (DFT) combined with dynamical mean-field theory, **revealing a formation of local moments on Cr from strong local Coulomb interactions**. We show that the presence of local dynamical correlations leads to a modification of the electronic structure of ferromagnetically ordered CrI_3 . In contrast to conventional DFT+ U calculations, we find that the top of the valence band in ML CrI_3 demonstrates essentially different orbital character for minority and majority spin states, which is closer to the standard DFT results. This leads to a strong spin polarization of the optical conductivity upon hole doping, which could be verified experimentally.

DOI: [10.1103/PhysRevB.105.205124](https://doi.org/10.1103/PhysRevB.105.205124)

PHYSICAL REVIEW B **104**, 155109 (2021)

Electronic structure of chromium trihalides beyond density functional theory

Swagata Acharya,^{1,*} Dimitar Pashov,² Brian Cunningham,³ Alexander N. Rudenko,¹ Malte Rösner,¹ Myrta Grüning,⁴

Mark van Schilfgaarde,^{2,5} and Mikhail I. Katsnelson¹

¹Institute for Molecules and Materials, Radboud University, NL-6525 AJ Nijmegen, The Netherlands


²King's College London, Theory and Simulation of Condensed Matter, The Strand, WC2R 2LS London, United Kingdom

³Centre for Theoretical Atomic, Molecular and Optical Physics,

Queen's University Belfast, Belfast BT71NN, Northern Ireland, United Kingdom

⁴Atomistic Simulation Centre, Queen's University Belfast, Belfast BT71NN, Northern Ireland, United Kingdom

⁵National Renewable Energy Laboratory, Golden, Colorado 80401, USA

 (Received 16 June 2021; revised 28 August 2021; accepted 22 September 2021; published 5 October 2021)

We explore the electronic band structure of freestanding monolayers of chromium trihalides CrX_3 , $X = \text{Cl}, \text{Br}, \text{I}$, within an advanced *ab initio* theoretical approach based on the use of Green's function functionals. We compare the local density approximation with the quasiparticle self-consistent GW (QS \tilde{G} W) approximation and its self-consistent extension (QS \tilde{G} \tilde{W}) by solving the particle-hole ladder Bethe-Salpeter equations to improve the effective interaction W . We show that, at all levels of theory, the valence band consistently changes shape in the sequence $\text{Cl} \rightarrow \text{Br} \rightarrow \text{I}$, and the valence band maximum shifts from the M point to the Γ point. **By analyzing the dynamic and momentum-dependent self-energy, we show that QS \tilde{G} \tilde{W} adds to the localization of the systems in comparison with QS \tilde{G} W, thereby leading to a narrower band and reduced amount of halogens in the valence band manifold.** Further analysis shows that $X = \text{Cl}$ is most strongly correlated, and $X = \text{I}$ is least correlated (most bandlike) as the hybridization between Cr d and X p enhances in the direction $\text{Cl} \rightarrow \text{Br} \rightarrow \text{I}$. For CrBr_3 and CrI_3 , we observe remarkable differences between the QS \tilde{G} W and QS \tilde{G} \tilde{W} valence band structures, while their eigenfunctions are very similar. We show that weak perturbations, like moderate strain, weak changes to the d - p hybridization, and adding small U , can flip the valence band structures between these two solutions in these materials.

DOI: [10.1103/PhysRevB.104.155109](https://doi.org/10.1103/PhysRevB.104.155109)

Candidate materials Fe_3GeTe_2 have strong correlation

npj | computational
materials

www.nature.com/npjcomputat

PHYSICAL REVIEW B **93**, 144404 (2016)

ARTICLE OPEN

Fe_3GeTe_2 : a site-differentiated Hund metal

Taek Jung Kim^{1,3}, Siheon Ryee^{1,2,3} and Myung Joon Han^{1,3}

Magnetism in two-dimensional (2D) van der Waals (vdW) materials has lately attracted considerable attention from the point of view of both fundamental science and device applications. Obviously, establishing a detailed and solid understanding of their magnetism is the key first step toward various applications. Although Fe_3GeTe_2 is a representative ferromagnetic (FM) metal in this family, many aspects of its magnetic and electronic behaviors still remain elusive. Here, we report our new finding that Fe_3GeTe_2 is a special type of correlated metal known as “Hund metal”. Furthermore, we demonstrate that Hund metallicity in this material is quite unique by exhibiting remarkable site dependence of Hund correlation strength, hereby dubbed “site-differentiated Hund metal”. Within this new picture, many of the previous experiments can be clearly understood, including the ones that were seemingly contradictory to one another.

npj Computational Materials (2022)8:245; <https://doi.org/10.1038/s41524-022-00937-x>



Electronic correlation and magnetism in the ferromagnetic metal Fe_3GeTe_2

Zhu,^{1,*} Marc Janoschek,¹ D. S. Chaves,^{2,†} J. C. Cezar,² Tomasz Durakiewicz,¹ Filip Ronning,¹ Yasmine Sassa,³ Martin Mansson,^{4,5} B. L. Scott,¹ N. Wakeham,¹ Eric D. Bauer,¹ and J. D. Thompson^{1,‡}

¹Los Alamos National Laboratory, Los Alamos, New Mexico 87545, USA

²Synchrotron Light Laboratory (LNLS), National Center for Research in Energy and Materials (CNPEM), Campinas, Brazil

³Uppsala University, Department of Physics & Astronomy, S-75121 Uppsala, Sweden

⁴Laboratory for Neutron Scattering and Imaging, Paul Scherrer Institute, CH-5232 Villigen PSI, Switzerland
⁵Department of Materials and Nanophysics, KTH Royal Institute of Technology, SE-16440 Stockholm Kista, Sweden

(Received 17 December 2015; published 5 April 2016)

Motivated by the search for design principles of rare-earth-free strong magnets, we present a study of electronic structure and magnetic properties of the ferromagnetic metal Fe_3GeTe_2 within the local-density approximation (LDA) of the density-functional theory, and its combination with dynamical mean-field theory (DMFT). To compare these calculations, we measure magnetic and thermodynamic properties as well as x-ray magnetic circular dichroism and the photoemission spectrum of single-crystal Fe_3GeTe_2 . We find that the experimentally determined Sommerfeld coefficient is enhanced by an order of magnitude with respect to the LDA value. This enhancement can be partially explained by LDA+DMFT. In addition, the inclusion of dynamical electronic correlation effects provides the experimentally observed magnetic moments, and the spectral density is in better agreement with photoemission data. **These results establish the importance of electronic correlations in this ferromagnet.**

DOI: [10.1103/PhysRevB.93.144404](https://doi.org/10.1103/PhysRevB.93.144404)

Spin structures in Fe_3GeTe_2

Magnetic skyrmions in Fe_5GeTe_2

communications physics

ARTICLE

<https://doi.org/10.1038/s42005-022-01031-w> OPEN

Skyrmionic spin structures in layered Fe_5GeTe_2 up to room temperature

Maurice Schmitt¹, Thibaud Denneulin², András Kovács², Tom G. Sanderson^{1,3}, Philipp Rübmann^{3,4}, Aga Shahee^{1,10}, Tanja Scholz⁵, Amir H. Tavabi², Martin Gradhand^{1,6}, Phivos Mavropoulos⁷, Bettina V. Lotsch^{5,8}, Rafal E. Dunin-Borkowski², Yuriy Mokrousov^{1,3}, Stefan Blügel³ & Matthias Kläui^{1,9,✉}

The role of the crystal lattice, temperature and magnetic field for the spin structure formation in the 2D van der Waals magnet Fe_5GeTe_2 with magnetic ordering up to room temperature is a key open question. Using Lorentz transmission electron microscopy, we experimentally observe topological spin structures up to room temperature in the metastable pre-cooling and stable post-cooling phase of Fe_5GeTe_2 . Over wide temperature and field ranges, skyrmionic magnetic bubbles form without preferred chirality, which is indicative of centrosymmetry. These skyrmions can be observed even in the absence of external fields. To understand the complex magnetic order in Fe_5GeTe_2 , we compare macroscopic magnetometry characterization results with microscopic density functional theory and spin-model calculations. Our results show that even up to room temperature, topological spin structures can be stabilized in centrosymmetric van der Waals magnets.

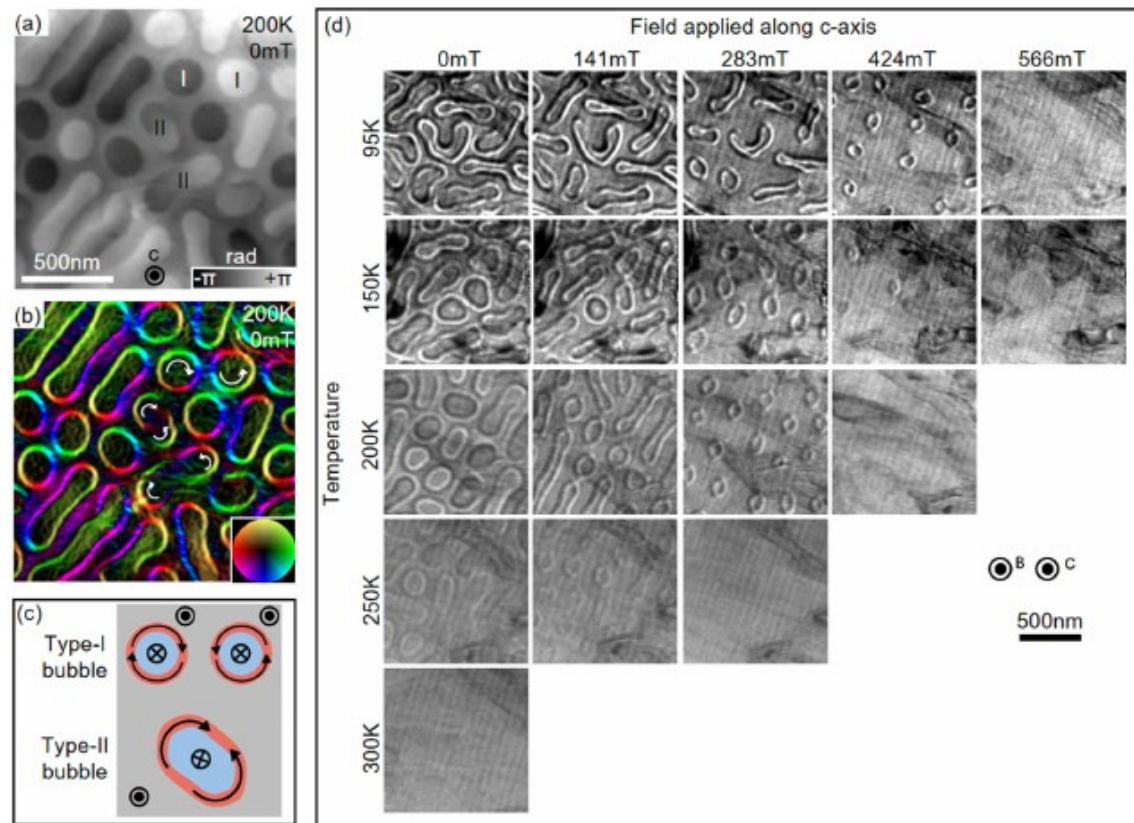


Fig. 2 Magnetic imaging of Fe_5GeTe_2 in the pre-cooling phase, revealing skyrmionic spin structures. **a** Phase shift image obtained using off-axis electron holography at $T = 200$ K and $B = 0$ mT in Fe_5GeTe_2 with the c -axis perpendicular to the image plane after previously applying out-of-plane fields up to $B = 566$ mT. **b** Corresponding color-coded magnetic induction map where the direction of the magnetic field is given by the color wheel. Type-II as well as type-I bubbles with opposite winding numbers are present. **c** Schematic illustration of type-I and type-II bubbles. **d** Series of Fresnel images taken at various temperatures and external out-of-plane fields (parallel to the c -axis) with a defocus of -1 nm, in a ≈ 100 nm thick plan-view lamella (c -axis is perpendicular to the image plane). The magnetization within the magnetic bubbles opposes the external field, whereas the areas the magnetization between the bubbles are parallel to the field. Bubbles begin to form at higher external fields for lower temperatures.

Chiral Spin Spirals at the Surface of the van der Waals Ferromagnet Fe_3GeTe_2

Mariëlle J. Meijer^{*}, Juriaan Lucassen, Rembert A. Duine, Henk J.M. Swagten, Bert Koopmans, Reinoud Lavrijsen, and Marcos H. D. Guimarães^{*}

✓ Cite this: *Nano Lett.* 2020, 20, 12, 8563–8568

Publication Date: November 25, 2020

<https://doi.org/10.1021/acs.nanolett.0c03111>

Copyright © 2022 American Chemical Society. This publication is licensed under [CC-BY-NC-ND](#).

Open Access

Article Views

5622

Altmetric

4

Citations

27

[LEARN ABOUT THESE METRICS](#)

Nano Letters

pubs.acs.org/NanoLett

Letter

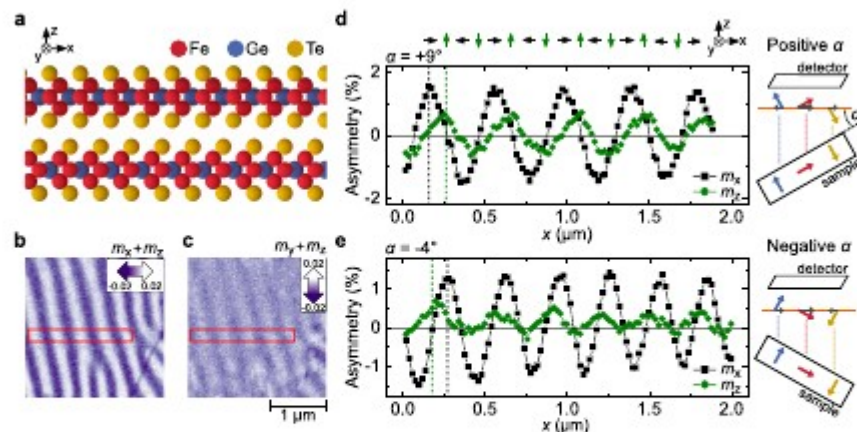


Figure 1. Spin spirals at the surface of a $d = 185$ nm thick FGT flake at $T = 150$ K. (a) Crystal structure of two FGT layers. (b, c) SEMPA images measured at the surface of FGT for $\alpha = +9^\circ$. Panel (b) shows m_x contrast and panel (c) m_y for the exact same area, with the color scale (in arbitrary units) indicated by the arrows in the top right-hand corner. Additionally, in both SEMPA images an out-of-plane magnetization m_z can be present, which is adjustable in panel (c) only. (d, e) Averaged magnetization profiles obtained from SEMPA measurements for the same area. In black and green we depict the average magnetization profile in the red rectangle of panels (b) and (c), respectively. The sample tilt, illustrated on the right, was $\alpha = +9^\circ$ in panel (d) and $\alpha = -4^\circ$ in panel (e). The phase shift reverses from $+\pi/2$ in panel (d) to $-\pi/2$ in panel (e), which is expected for a m_x magnetization contrast in the SEMPA image in panel (c). Overall, we observe a counterclockwise rotating Néel spin spiral as is indicated schematically by the arrows above panel (d).



Creation of skyrmions in van der Waals ferromagnet Fe_3GeTe_2 on $(\text{Co}/\text{Pd})_n$ superlattice

M. YANG¹, Q. LI¹, R. V. CHOPDEKAR², R. DHALL¹, J. TURNER¹, J. D. CARLSTRÖM¹, C. OPHUS¹, C. KLEWE, P. SHAFER¹, [] AND Z. Q. QIU¹

+6 authors [Authors Info & Affiliations](#)

SCIENCE ADVANCES · 4 Sep 2020 · Vol 6, Issue 36 · DOI:10.1126/sciadv.abb5157

4,038 66



Abstract

Magnetic skyrmions are topological spin textures, which usually exist in noncentrosymmetric materials where the crystal inversion symmetry breaking generates the so-called Dzyaloshinskii-Moriya interaction. This requirement unfortunately excludes many important magnetic material classes, including the recently found two-dimensional van der Waals (vdW) magnetic materials, which offer unprecedented opportunities for spintronic technology. Using photoemission electron microscopy and Lorentz transmission electron microscopy, we investigated and stabilized Néel-type magnetic skyrmion in vdW ferromagnetic Fe_3GeTe_2 on top of $(\text{Co}/\text{Pd})_n$ in which the Fe_3GeTe_2 has a centrosymmetric crystal structure. We demonstrate that the magnetic coupling between the Fe_3GeTe_2 and the $(\text{Co}/\text{Pd})_n$ could create skyrmions in Fe_3GeTe_2 without the need of an external magnetic field. Our results open exciting opportunities in spintronic research and the engineering of topologically protected nanoscale features by expanding the group of skyrmion host materials to include these previously unknown vdW magnets.

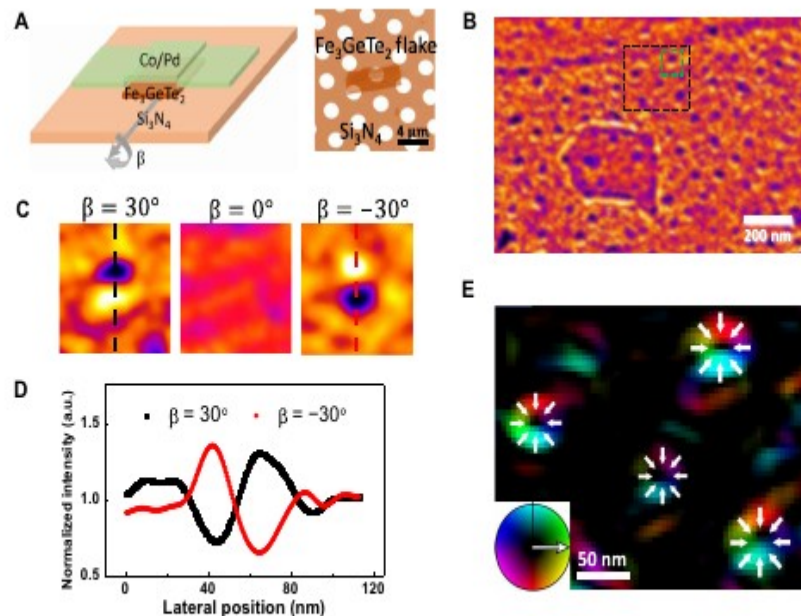


Fig. 3. Néel-type skyrmions observed by LTEM in the system of FGT/ $(\text{Co}/\text{Pd})_{10}$ multilayers. (A) Schematic drawing of sample structure and TEM image of FGT flake on a porous Si_3N_4 membrane. The thickness of FGT flake here is 70 nm. (B) LTEM images of FGT/ $(\text{Co}/\text{Pd})_{10}$ at a sample tilting angle of 30° . (C) LTEM images taken from selected area in (B) (green dashed box) at sample tilting angles of 30° , 0° , and -30° . The zero contrast at 0° tilting angle and the reversed contrasts at opposite tilting angles indicate the Néel-type structure of the skyrmion. All LTEM measurements were performed at liquid nitrogen temperature. (D) Line profiles of the contrast from the same skyrmion at opposite tilting angles, showing the contrast reversal of the Néel-type skyrmion at opposite tilting angles. (E) The magnetization distribution obtained by exit wave phase reconstruction of the selected LTEM data [black dashed box in (B)]. The white arrows and the color wheel indicate the in-plane direction of the magnetization.

Observation of Magnetic Skyrmion Bubbles in a van der Waals Ferromagnet Fe_3GeTe_2

Bei Ding,^{†,||,⊥} Zefang Li,^{†,||,⊥} Guizhou Xu,^{†,⊥} Hang Li,^{†,||} Zhipeng Hou,[§] Enke Liu,[†] Xuekui Xi,[†] Feng Xu,[†] Yuan Yao,[†] and Wenhong Wang*^{†,⊥}

[†]Beijing National Laboratory for Condensed Matter Physics, Institute of Physics, Chinese Academy of Sciences, Beijing 100190, China

[‡]School of Materials Science and Engineering, Nanjing University of Science and Technology, Nanjing 210094, China

[§]South China Academy of Advanced Optoelectronics, South China Normal University, Guangzhou 510006, China

^{||}University of Chinese Academy of Sciences, Beijing 100049, China

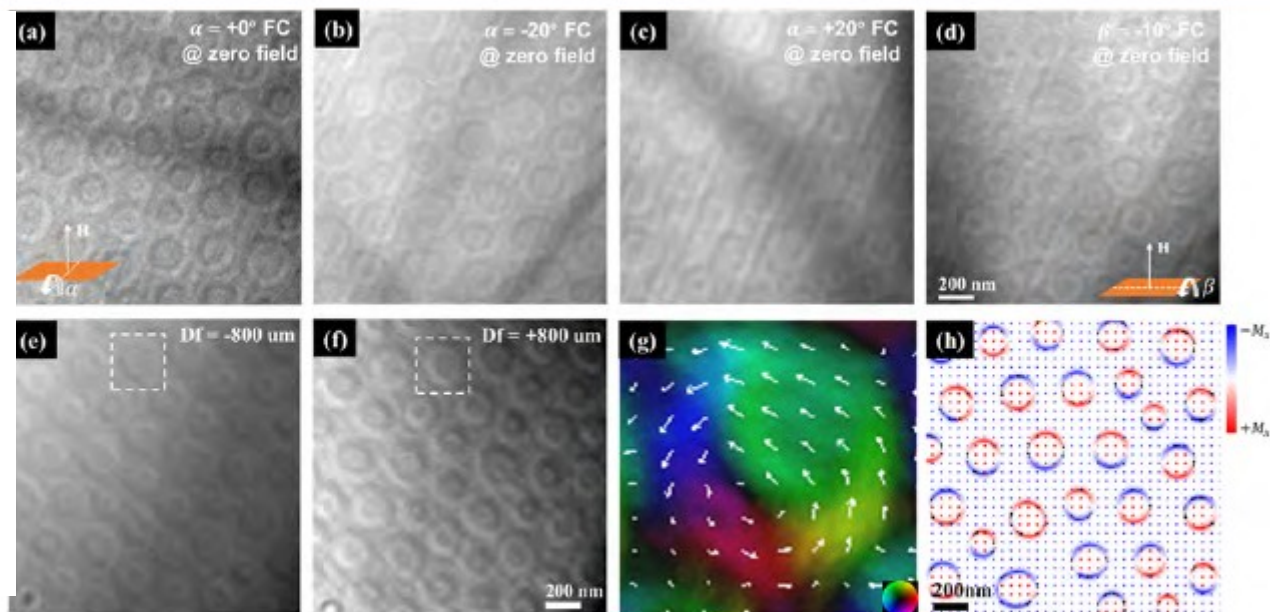


Figure 4. (a–d) Underfocused Lorentz-TEM image of skyrmion bubbles at 93 K after FC manipulation with a field (600 Oe) applied with rotation angles. (α ; as shown schematically in the inset of (a) $\alpha = -20^\circ$, (b) $\alpha = 0^\circ$, (c) $\alpha = +20^\circ$, and (d) $\beta = -10^\circ$, respectively). (e, f) Underfocused and overfocused Lorentz-TEM images of the skyrmion bubbles taken at 93 K and in zero-field. (g) An enlarged in-plane magnetization distribution map obtained by TIE analysis for a selected skyrmion bubble indicated by the white dotted box in parts e and f. The white arrows represent the magnetization direction at each point, and the color wheel is in the right corner. (h) Theoretical simulation of skyrmion lattices at an applied magnetic field with 600 Oe for $\alpha = 0^\circ$. The in-plane magnetization distribution is represented by blue ($-M_z$) and red ($+M_z$) regions. The scale bar is 200 nm.

Spin structures in Cr-X₃

Topological spin texture in Janus monolayers of the chromium trihalides $\text{Cr}(\text{I}, \text{X})_3$

Changsong Xu^{1,*}, Junsheng Feng,^{2,3,*} Sergei Prokhorenko,¹ Yousra Nahas,¹ Hongjun Xiang,^{3,4,†} and L. Bellaïche^{1,‡}

¹Physics Department and Institute for Nanoscience and Engineering, University of Arkansas, Fayetteville, Arkansas 72701, USA

²School of Physics and Materials Engineering, Hefei Normal University, Hefei 230601, People's Republic of China

³Key Laboratory of Computational Physical Sciences (Ministry of Education), State Key Laboratory of Surface Physics, and Department of Physics, Fudan University, Shanghai 200433, People's Republic of China

⁴Collaborative Innovation Center of Advanced Microstructures, Nanjing 210093, People's Republic of China



(Received 25 July 2019; revised manuscript received 18 September 2019; accepted 28 January 2020; published 10 February 2020)

Topological magnetic states are promising for ultradense memory and logic devices. Recent progress in two-dimensional magnets encourages the idea to realize topological states, such as skyrmions and merons, in freestanding monolayers. However, monolayers such as CrI_3 lack Dzyaloshinskii-Moriya interactions (DMIs) and thus do not naturally exhibit skyrmions/merons but rather a ferromagnetic state. Here we propose the fabrication of $\text{Cr}(\text{I}, \text{X})_3$ Janus monolayers, in which the Cr atoms are covalently bonded to the underlying I ions and top-layer Br or Cl atoms. By performing first-principles calculations and Monte Carlo simulations, we identify strong enough DMIs, which leads to not only helical cycloid phases, but also to topologically nontrivial states, such as the intrinsic domain wall skyrmions in $\text{Cr}(\text{I}, \text{Br})_3$ and the magnetic-field-induced bimerons in $\text{Cr}(\text{I}, \text{Cl})_3$. Microscopic origins of such spin textures are revealed as well.

DOI: [10.1103/PhysRevB.101.060404](https://doi.org/10.1103/PhysRevB.101.060404)

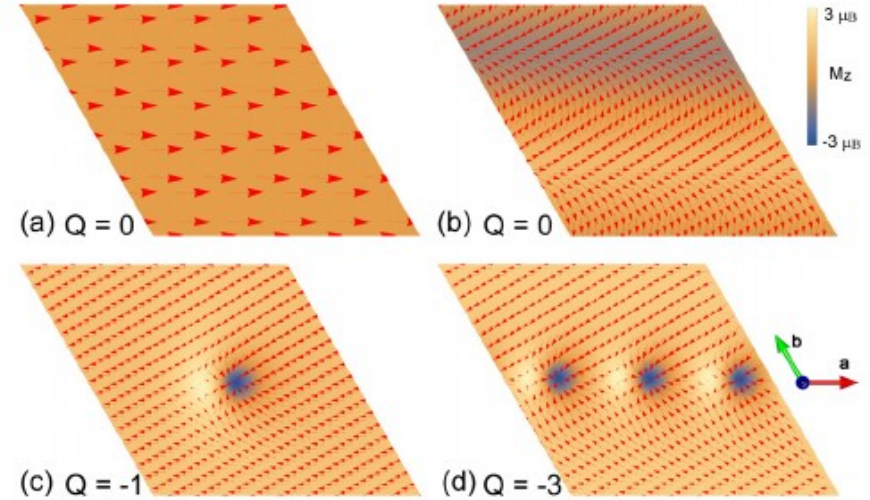


FIG. 3. Magnetic structures and topological charges of $\text{Cr}(\text{I}, \text{Cl})_3$. (a) shows the in-plane zigzag-canted FM state; (b) illustrates the in-plane cycloidal structure; (c) and (d) display one and three bimerons, respectively, with an out-of-plane magnetic field B of 0.8 T. See Fig. 2 for explanations of the color map and the vectors.

Evidence of non-collinear spin texture in magnetic moiré superlattices

Hongchao Xie^{1,6}, Xiangpeng Luo^{1,6}, Zhipeng Ye^{2,6}, Zeliang Sun^{1,6}, Gaihua Ye², Suk Hyun Sung³, Haiwen Ge⁴, Shaohua Yan⁵, Yang Fu⁵, Shangjie Tian⁵, Hechang Lei⁵, Kai Sun¹, Robert Hovden³, Rui He² & Liuyan Zhao¹✉

Moiré magnetism is emerging as a platform to design and control exotic magnetic phases in twisted magnetic two-dimensional crystals. Non-collinear spin texture emerging from twisted two-dimensional magnets with collinear spins is one of the most profound consequences of moiré magnetism and forms the basis for realizing non-trivial magnetic orders and excitations. However, no direct experimental observations of non-collinear spins in moiré magnets have been made, despite recent theoretical and experimental efforts. Here, we report evidence of non-collinear spin texture in two-dimensional twisted double bilayer CrI₃. We distinguish the non-collinear spins with a gradual spin flop process from the collinear spins with sudden spin flip transitions and identify a net magnetization emerging from the collinear spins. We also demonstrate that both non-collinear spins and net magnetization are present at twist angles from 0.5° to 5° but are most prominent for 1.1°. We resolve a critical temperature of 25 K for the onset of the net magnetization and the softening of the non-collinear spins in the 1.1° samples. This is substantially lower than the Néel temperature of 45 K for natural few layers. Our results provide a platform to explore non-trivial magnetism with non-collinear spins.

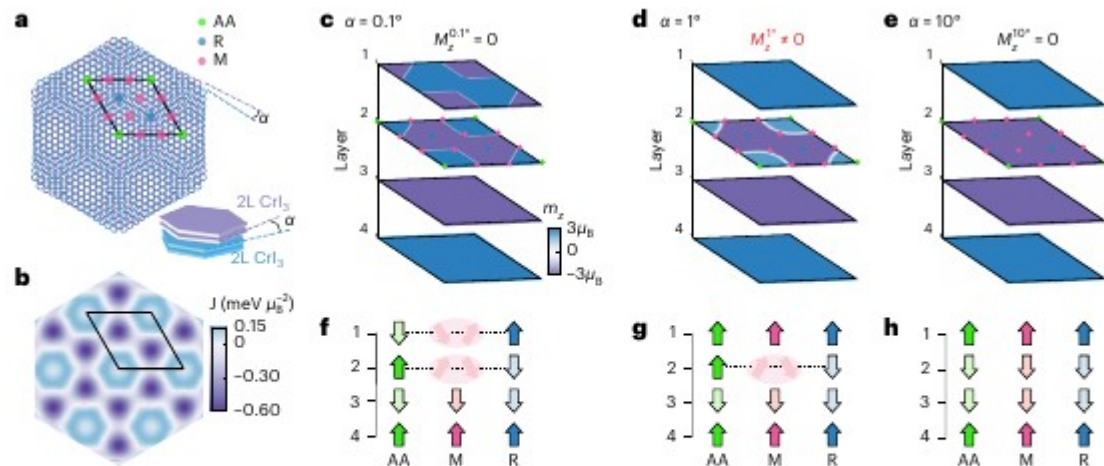


Fig. 1 | Calculations of the magnetic ground states of tDB CrI₃. **a**, The moiré superlattice formed at the interface between two 2L CrI₃, namely between the second and third layers. Regions of AA- (green), R- (blue) and M-type (red) stacking geometries are marked in one moiré supercell (black parallelogram). Inset: Schematic of twisting two 2L CrI₃ by an angle α . **b**, The periodically modulating interlayer exchange coupling J at the interface between two 2L CrI₃.

c–e, The calculated distributions of the out-of-plane magnetization M_z in a moiré supercell for all four layers of tDB CrI₃ at three representative twist angles of $\alpha = 0.1^\circ$ (**c**), 1° (**d**) and 10° (**e**), with zero, non-zero and zero total magnetization, respectively. **f–h**, Sketches of the calculated layered magnetism centring at AA (green), across M (red) and centring at R (blue) sites for the magnetic ground states in **c** (**f**), **d** (**g**) and **e** (**h**).

Curved Magnetism in CrI_3

Alexander Edström^{1,2}, Danila Amoroso^{3,4}, Silvia Picozzi,³ Paolo Barone⁵, and Massimiliano Stengel^{1,6}

¹Institut de Ciència de Materials de Barcelona (ICMAB-CSIC), Campus UAB, 08193 Bellaterra, Spain

²Department of Applied Physics, School of Engineering Sciences, KTH Royal Institute of Technology, AlbaNova University Center, 10691 Stockholm, Sweden

³Consiglio Nazionale delle Ricerche CNR-SPIN, c/o Università degli Studi 'G. D'Annunzio', 66100 Chieti, Italy

⁴NanoMat/Q-mat/CESAM, Université de Liège, B-4000 Liege, Belgium

⁵Consiglio Nazionale delle Ricerche CNR-SPIN, Area della Ricerca di Tor Vergata, Via del Fosso del Cavaliere 100, I-00133 Rome, Italy

⁶ICREA—Institutio Catalana de Recerca i Estudis Avançats, 08010 Barcelona, Spain

(Received 28 October 2021; revised 8 March 2022; accepted 7 April 2022; published 28 April 2022)

Curved magnets attract considerable interest for their unusually rich phase diagram, often encompassing exotic (e.g., topological or chiral) spin states. Micromagnetic simulations are playing a central role in the theoretical understanding of such phenomena; their predictive power, however, rests on the availability of reliable model parameters to describe a given material or nanostructure. Here we demonstrate how noncollinear-spin polarized density-functional theory can be used to determine the flexomagnetic coupling coefficients in real systems. By focusing on monolayer CrI_3 , we find a crossover as a function of curvature between a magnetization normal to the surface to a cycloidal state, which we rationalize in terms of effective anisotropy and Dzyaloshinskii-Moriya contributions to the magnetic energy. Our results reveal an unexpectedly large impact of spin-orbit interactions on the curvature-induced anisotropy, which we discuss in the context of existing phenomenological models.

DOI: 10.1103/PhysRevLett.128.177202

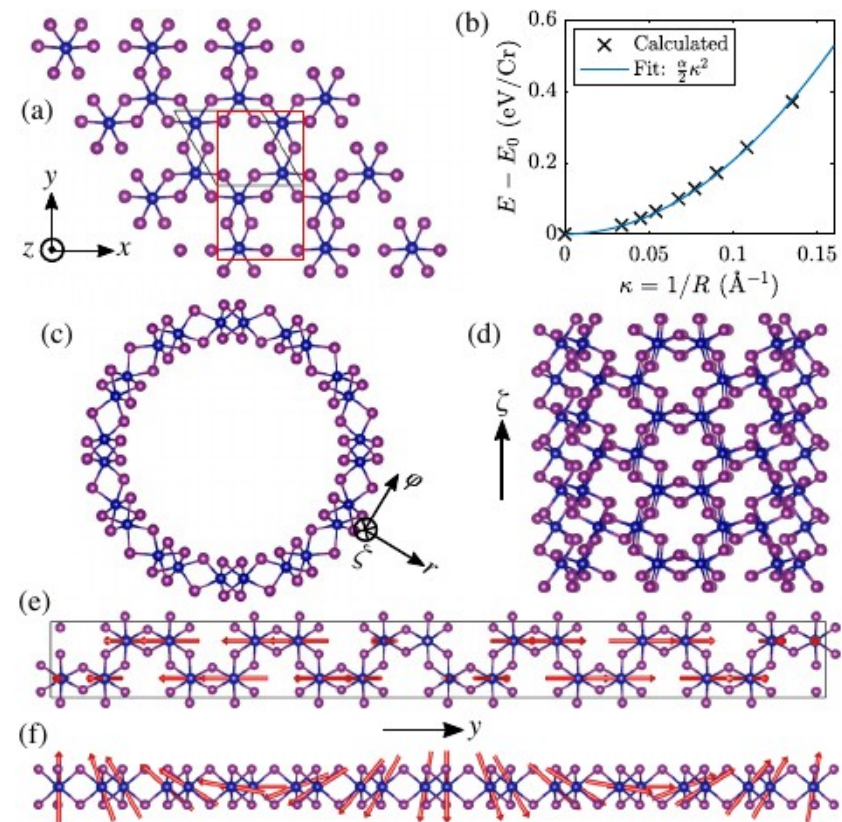


FIG. 1. (a) Monolayer CrI_3 (Cr, blue; I, purple) with black lines showing the primitive 8 atom unit cell (2 Cr and 6 I) while the red lines show the doubled unit cell, N of which are used to construct (N, N) NTs. (b) Calculated energy (per Cr) as a function of curvature. (c) $N = 6$ NT from above and (d) side. (e) Supercell strip for a spin spiral with wavelength equal to the circumference of the $N = 6$ NT, seen from above and (f) side, with arrows showing the magnetic moments $\mathbf{m}_i = [0, -\sin(qy_i), \cos(qy_i)]$.

Magnetic skyrmions in atomic thin CrI₃ monolayer F

Cite as: Appl. Phys. Lett. **114**, 232402 (2019); doi: [10.1063/1.5096782](https://doi.org/10.1063/1.5096782)

Submitted: 19 March 2019 · Accepted: 27 April 2019 ·

Published Online: 10 June 2019



Aroop K. Behera,¹ Sugata Chowdhury,² and Suprem R. Das^{1,3,a)}

AFFILIATIONS

¹Industrial and Manufacturing Systems Engineering, Kansas State University, Manhattan, Kansas 66506, USA

²Department of Chemical and Biomolecular Engineering, Rice University, Houston, Texas 77251, USA

³Electrical and Computer Engineering, Kansas State University, Manhattan, Kansas 66506, USA

^{a)}Author to whom correspondence should be addressed: srdas@ksu.edu

ABSTRACT

In this letter, we report on the visualization of topologically protected spin textures, in the form of magnetic skyrmions, in recently discovered monoatomic-thin two-dimensional CrI₃. By combining density functional theory and atomistic spin dynamic simulation, we demonstrate that an application of an out-of-plane electric field to the CrI₃ lattice favors the formation of sub-10 nm skyrmions at 0 K temperature. The spin texture arises due to a strong correlation between magnetocrystalline anisotropy, Dzyaloshinskii-Moriya interaction, and the vertical electric field, whose shape and size could be tuned with the magnetic field. Such a finding will open avenues for atomic-scale quantum engineering and precision sensing.

Published under license by AIP Publishing. <https://doi.org/10.1063/1.5096782>

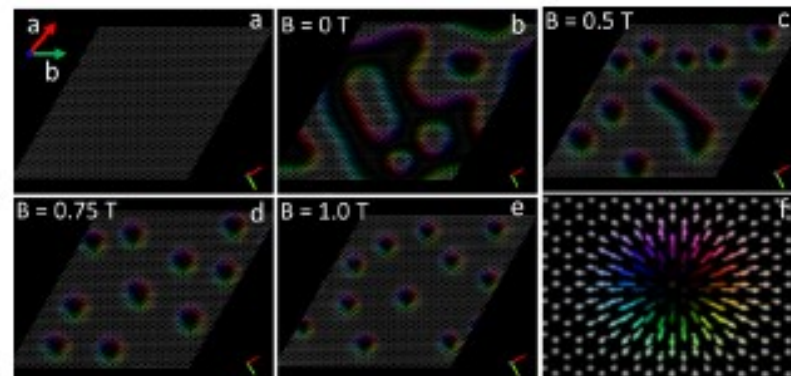


FIG. 3. CrI₃ spin lattice for the atomistic spin dynamics calculation. (a) The magnetic moments of Cr atoms are arranged in a honeycomb graphenelike geometry. The white color indicates spin alignment in the +z direction, the bottom right inset shows the spin orientation color map, and the top left inset shows the crystallographic axes. Figure (b)–(e) show the spin dynamics calculation (LLG) in the ground state configuration of spins at various magnetic fields when CrI₃ undergoes a vertical electric field of 1.2 V/nm and with a hypothetical ~70% reduced anisotropy, forming a mixture of chiral domains and skyrmions to pure skyrmionic states. Figure (f) shows a magnified view.

Moiré Skyrmions and Chiral Magnetic Phases in Twisted CrX_3 ($X = \text{I, Br, and Cl}$) Bilayers

Muhammad Akram, Harrison LaBollita, Dibyendu Dey, Jesse Kapeghian, Onur Erten*, and Antia S. Botana*

Cite this: *Nano Lett.* 2021, 21, 15, 6633–6639

Publication Date: August 2, 2021

<https://doi.org/10.1021/acs.nanolett.1c02096>

Copyright © 2021 American Chemical Society

[Request reuse permissions](#)

Article Views | Altmetric | Citations

3213

1

37

[LEARN ABOUT THESE METRICS](#)

Share | Add to | Export

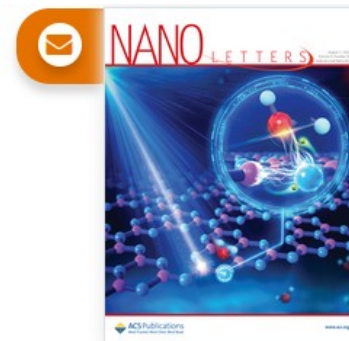


Read Online

PDF (1 MB)

SI

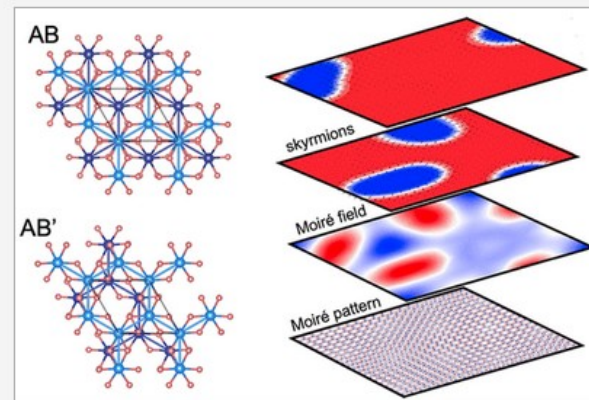
Supporting Info (1) »

SUBJECTS: Energy, Layered materials, Layers, Magnetic properties, Vesicles


Nano Letters

Abstract


We present a comprehensive theory of the magnetic phases in twisted bilayer chromium trihalides through a combination of first-principles calculations and atomistic simulations. We show that the stacking-dependent interlayer exchange leads to an effective moiré field that is mostly ferromagnetic with antiferromagnetic patches. A wide range of noncollinear magnetic phases can be stabilized as a function of the twist angle and Dzyaloshinskii–Moriya interaction as a result of the competing interlayer antiferromagnetic coupling and the energy cost for forming domain walls. In particular, we demonstrate that for small twist angles various skyrmion crystal phases can be stabilized in both CrI_3 and CrBr_3 . Our results provide an interpretation for the recent observation of noncollinear magnetic phases in twisted bilayer CrI_3 and demonstrate the possibility of engineering further nontrivial magnetic ground states in twisted bilayer chromium trihalides.



Skyrmions in twisted van der Waals magnets

 Muhammad Akram  and Onur Erten

Department of Physics, Arizona State University, Box 871504, Tempe, Arizona 85287-1504, USA

 (Received 8 August 2020; revised 17 March 2021; accepted 31 March 2021; published 13 April 2021)

Magnetic skyrmions in two-dimensional (2D) chiral magnets are often stabilized by a combination of a Dzyaloshinskii-Moriya interaction and an external magnetic field. Here, we show that skyrmions can also be stabilized in twisted moiré superlattices with a Dzyaloshinskii-Moriya interaction in the absence of an external magnetic field. Our setup consists of a 2D ferromagnetic layer twisted on top of an antiferromagnetic substrate. The coupling between the ferromagnetic layer and the substrate generates an effective alternating exchange field. We find a large region of the skyrmion crystal phase when the length scales of the moiré periodicity and skyrmions are compatible. Unlike chiral magnets under a magnetic field, skyrmions in moiré superlattices show an enhanced stability for the easy-axis (Ising) anisotropy which can be essential to realize skyrmions since most van der Waals magnets possess easy-axis anisotropy.

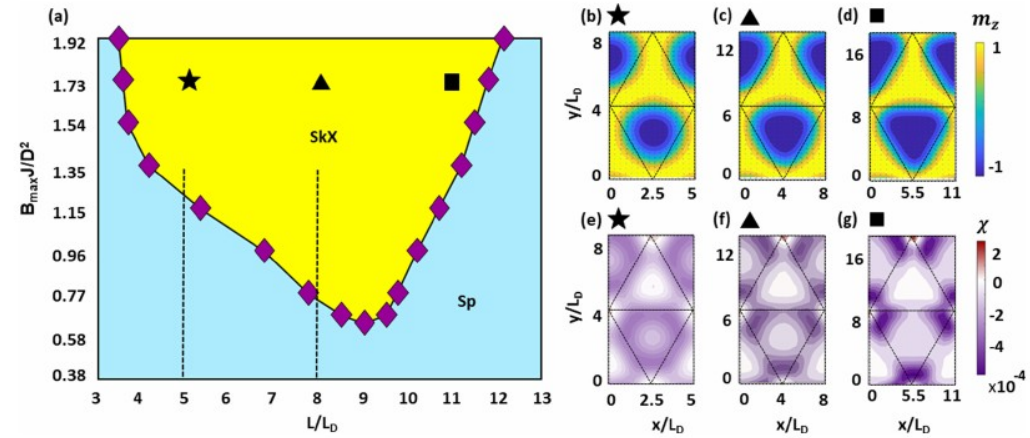
 DOI: [10.1103/PhysRevB.103.L140406](https://doi.org/10.1103/PhysRevB.103.L140406)


FIG. 2. $A = 0$ phase diagram at different moiré periods and exchange field. (a) Moiré period L vs maximum interlayer exchange field B_{\max} phase diagram with spiral (Sp) and skyrmion crystal (SkX) phases. Here, $L_D = (J/D)a$, where a is the lattice constant and the purple diamonds correspond to error bars. The dashed lines at $L = 5L_D$ and $L = 8L_D$ represent the cross sections of Figs. 3(a) and 5, respectively. (b)–(d) Magnetization texture and (e)–(g) topological charge density in 1×2 moiré supercells for $L/L_D = (5, 8, 11)$ and $B_{\max} J/D^2 = 1.73$ as marked by the \star , \blacktriangle , \blacksquare symbols in (a). The colors represent an out-of-plane component (m_z) of magnetization and topological charge density (χ) in (b)–(d) and (e)–(g), respectively. The arrows show the in-plane component of magnetization in (b)–(d) and the dotted lines represent 1×2 moiré supercells in (b)–(g).

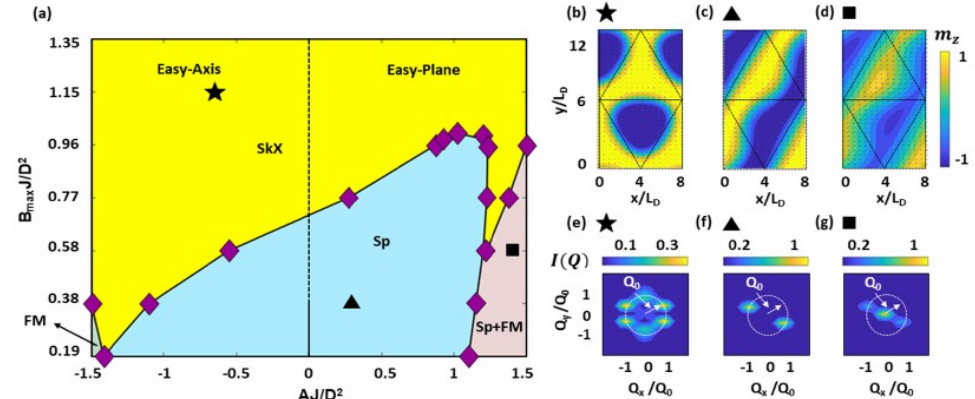
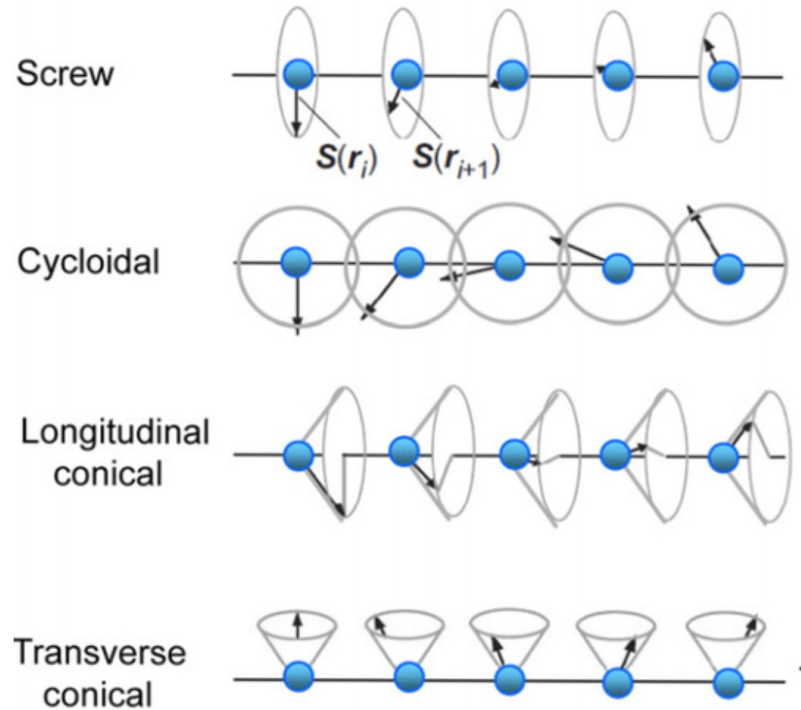
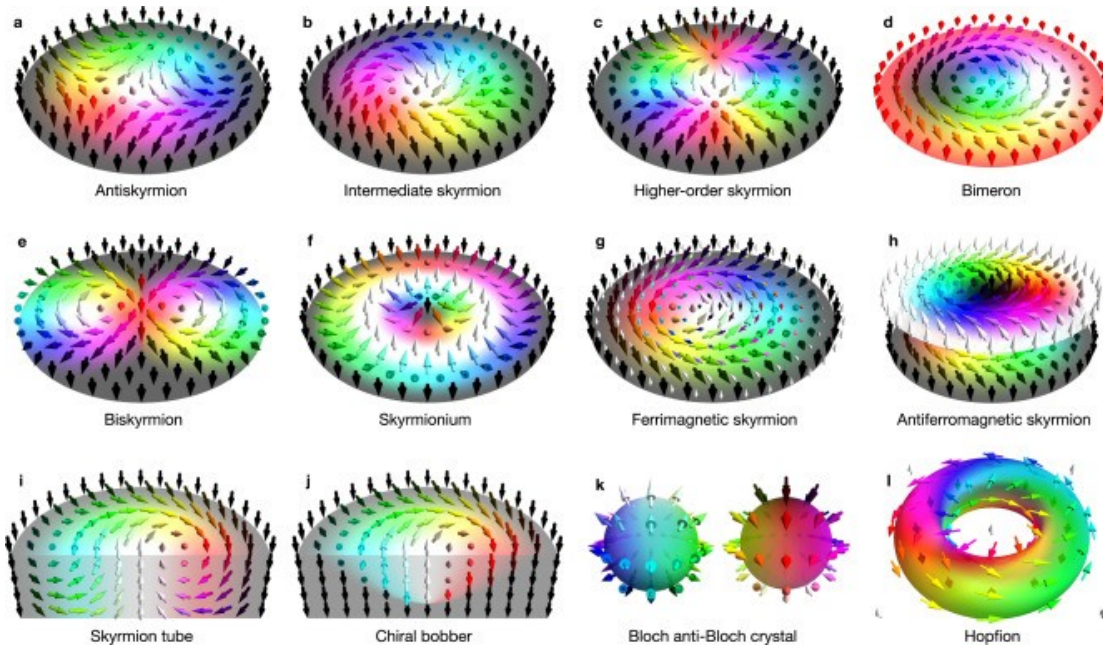


FIG. 3. $L = 8L_D$ phase diagram. (a) Anisotropy A vs maximum interlayer exchange field B_{\max} phase diagram with ferromagnetic (FM), spiral (Sp), skyrmion crystal (SkX), and mixed state (Sp + FM). Here, $L_D = (J/D)a$, where a is the lattice constant. (b)–(d) Magnetization texture in 1×2 moiré supercells and (e)–(g) spin structure factor for (\star , \blacktriangle , \blacksquare) symbols marked in (a). The parameters corresponding to these symbols are as follows: $\star = \{A = -0.6D^2/J, B_{\max} = 1.15D^2/J\}$, $\blacktriangle = \{A = 0.3D^2/J, B_{\max} = 0.38D^2/J\}$, and $\blacksquare = \{A = 1.14D^2/J, B_{\max} = 0.58D^2/J\}$.

Zoo of spin structures in vdW magnets



Strong evidence of two general properties of vdW materials

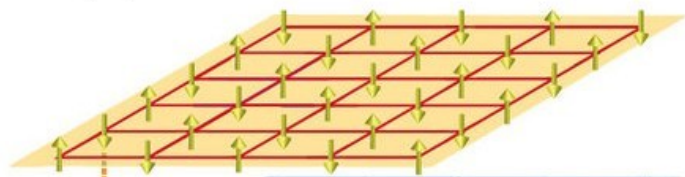
Strong Correlation

Non collinear spin structures

The Hamiltonian

$$H = - \sum_{ij\sigma} \left(t_{ij} + \frac{3J}{4} \delta_{ij} \right) c_{i\sigma}^\dagger c_{j\sigma} + J \sum_i \hat{\mathbf{S}}_i \cdot (c_{i\sigma}^\dagger \vec{\sigma}_{\sigma\sigma'} c_{i\sigma'}).$$

Here, $c_{i\sigma}^\dagger$ creates an electron with the spin σ on site i . $J > 0$ stands for the exchange coupling constant. $\vec{\sigma}$ is the vector of the Pauli spin matrices. The external magnetic moments $\hat{\mathbf{S}}_i$ are the generators of the $su(2)$ algebra in the lowest ($s = 1/2$) representation. The hopping term is modified by adding an extra J -dependent term to guarantee a finite $J \rightarrow +\infty$ limit [5]. Within a mean-field treatment the spatial spin structure is encoded in $\langle \hat{\mathbf{S}}_i \rangle = S \cdot \vec{n}_i$. Here, S is a localized spin magnitude, whereas a classical static vector \vec{n}_i determines a varying direction of the localized spin.



At large U limit Hamiltonian is simple

This approach proves effective in studying strongly correlated electrons. This can be seen as follows. At infinitely large Kondo coupling J , Eq. (1) goes over into the $U = \infty$ Hubbard model Hamiltonian [5],

$$H_{U=\infty} = - \sum_{ij\sigma} t_{ij} \tilde{c}_{i\sigma}^\dagger \tilde{c}_{j\sigma}. \quad (2)$$

The constrained electron operator $\tilde{c}_{i\sigma} = c_{i\sigma} (1 - n_{i\bar{\sigma}})$, where $n_{i\sigma} = c_{i\sigma}^\dagger c_{i\sigma}$ is the number operator, can be dynamically (in the effective action) factorized into the spinless charged fermionic f_i fields and the spinful bosonic z_i fields [12]. Inasmuch as $f_i^2 \equiv 0$, the local no double occupancy constraint that incorporates the strong electron correlations is rigorously implemented in this representation.

$$H_{U=\infty} = - \sum_{ij\sigma} t_{ij} \tilde{c}_{i\sigma}^\dagger \tilde{c}_{j\sigma}.$$

The partition function

$$Z = \int D\mu(z, f) \exp \mathcal{A}.$$

$$D\mu(z, f) = \prod_{i,t} \frac{2S}{2\pi i} \frac{d\bar{z}_i(t) dz_i(t)}{(1 + |z_i|^2)^2} d\bar{f}_i(t) df_i(t).$$

$$\mathcal{A} = \sum_i \int_0^\beta [ia_i^{(0)} - \bar{f}_i(\partial_t + ia_i^{(0)})f_i] dt - \int_0^\beta H dt.$$

The Action

$$\mathcal{A} = \sum_i \int_0^\beta [ia_i^{(0)} - \bar{f}_i(\partial_t + ia_i^{(0)})f_i] dt - \int_0^\beta H dt.$$

$$ia^{(0)} = -\langle z | \partial_t | z \rangle = S \frac{\dot{\bar{z}}z - \bar{z}\dot{z}}{1 + |z|^2},$$

$$H = -t \sum_{ij} \bar{f}_i f_j e^{ia_{ji}} + \text{H.c.} + \mu \sum_i \bar{f}_i f_i.$$

$$a_{ij} = -i \log \langle z_i | z_j \rangle, \quad \langle z_i | z_j \rangle = \frac{(1 + \bar{z}_i z_j)^{2S}}{(1 + |z_j|^2)^S (1 + |z_i|^2)^S}.$$

$$H = -t \sum_{ij} \bar{f}_i f_j e^{ia_{ji}} + \text{H.c.} + \mu \sum_i \bar{f}_i f_i.$$

$$a_{ji} = \phi_{ji} + i\chi_{ji}, \quad \bar{\phi}_{ji} = \phi_{ji}, \quad \bar{\chi}_{ji} = \chi_{ji}.$$

$$\phi_{ji} = iS \log \frac{1 + \bar{z}_i z_j}{1 + \bar{z}_j z_i}$$

$$= iS \log \frac{(S + S_i^z)(S + S_j^z) + S_i^- S_j^+}{(S + S_i^z)(S + S_j^z) + S_j^- S_i^+},$$

$$\chi_{ji} = -S \log \frac{(1 + \bar{z}_i z_j)(1 + \bar{z}_j z_i)}{(1 + |z_i|^2)(1 + |z_j|^2)}$$

$$= -S \log \left(\frac{\vec{S}_i \cdot \vec{S}_j}{2S^2} + \frac{1}{2} \right).$$

$$H = -t \sum_{ij} \bar{f}_i f_j e^{ia_{ji}} + \text{H.c.} + \mu \sum_i \bar{f}_i f_i.$$

$$a_{ji} = \phi_{ji} + i\chi_{ji}, \quad \bar{\phi}_{ji} = \phi_{ji}, \quad \bar{\chi}_{ji} = \chi_{ji}.$$

$$\phi_{ji} = iS \log \frac{1 + \bar{z}_i z_j}{1 + \bar{z}_j z_i}$$

$$= iS \log \frac{(S + S_i^z)(S + S_j^z) + S_i^- S_j^+}{(S + S_i^z)(S + S_j^z) + S_j^- S_i^+},$$

$$\chi_{ji} = -S \log \frac{(1 + \bar{z}_i z_j)(1 + \bar{z}_j z_i)}{(1 + |z_i|^2)(1 + |z_j|^2)}$$

$$= -S \log \left(\frac{\vec{S}_i \cdot \vec{S}_j}{2S^2} + \frac{1}{2} \right).$$

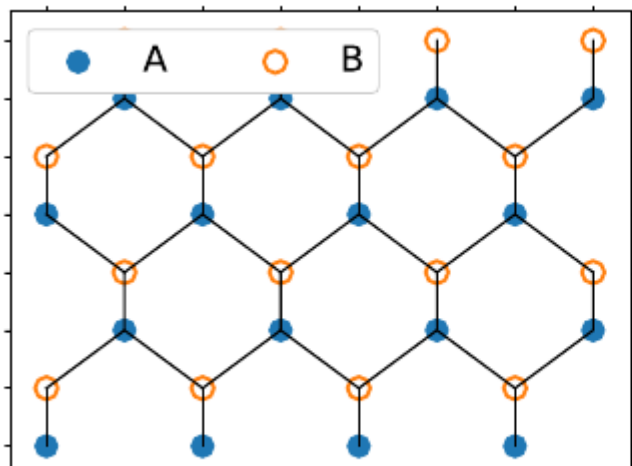
$$H = -t \sum_{\langle i,j \rangle} \bar{f}_i f_j e^{i\phi_{ji}} \left(\frac{\vec{S}_i \cdot \vec{S}_j}{2S^2} + \frac{1}{2} \right)^S + \mu \sum_i \bar{f}_i f_i.$$

$$H = -t \sum_{ij} \bar{f}_i f_j e^{ia_{ji}} + \text{H.c.} + \mu \sum_i \bar{f}_i f_i.$$

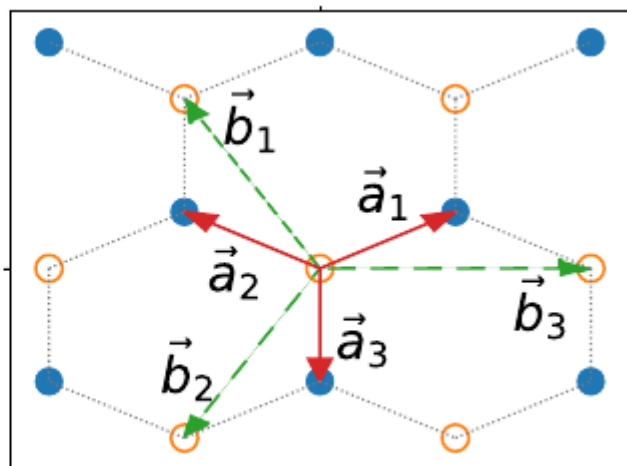


$$H = -t \sum_{\langle i,j \rangle} \bar{f}_i f_j e^{i\phi_{ji}} \left(\frac{\vec{S}_i \cdot \vec{S}_j}{2S^2} + \frac{1}{2} \right)^S + \mu \sum_i \bar{f}_i f_i.$$

$$H = -t \sum_{\langle i,j \rangle} \bar{f}_i f_j e^{i\phi_{ji}} \left(\frac{\vec{S}_i \cdot \vec{S}_j}{2S^2} + \frac{1}{2} \right)^S + \mu \sum_i \bar{f}_i f_i.$$

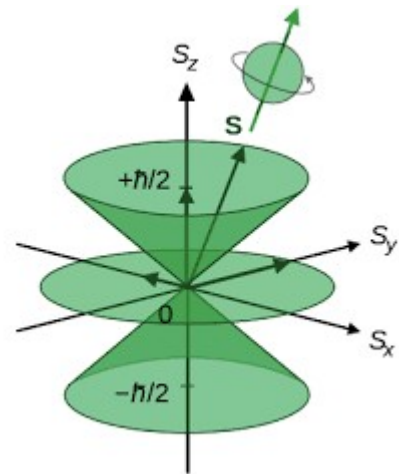


(a)




(b)

$$\vec{S}_i = (S_i^x, S_i^y, S_i^z) \equiv (\epsilon \cos \vec{q} \cdot \vec{r}_i, \epsilon \sin \vec{q} \cdot \vec{r}_i, \sqrt{S^2 - \epsilon^2}).$$



$$H = -t \sum_{\langle i,j \rangle} \bar{f}_i f_j e^{i\phi_{ji}} \left(\frac{\vec{S}_i \cdot \vec{S}_j}{2S^2} + \frac{1}{2} \right)^S + \mu \sum_i \bar{f}_i f_i.$$



$$H = -t_2 \sum_{i,j \in A} \bar{f}_i f_j \left(1 + i \frac{\epsilon^2}{S} \sin \frac{\vec{q} \cdot \vec{r}_{ij}}{2} e^{i\vec{q} \cdot \vec{r}_{ij}/2} \right) e^{-iS\vec{q} \cdot \vec{r}_{ij}} - t_2 \sum_{i,j \in B} \bar{f}_i f_j \left(1 - i \frac{\epsilon^2}{S} \sin \frac{\vec{q} \cdot \vec{r}_{ij}}{2} e^{-i\vec{q} \cdot \vec{r}_{ij}/2} \right) e^{iS\vec{q} \cdot \vec{r}_{ij}}$$

$$- t_1 \left(\frac{\epsilon}{S} \right)^{2S} \sum_{\substack{i \in A \\ j \in B}} \bar{f}_i f_j \left| \sin \frac{\vec{q} \cdot \vec{r}_{ij}}{2} \right|^{2S} + \text{H.c.}$$

Hopping from
site **A to A**

$$H = -t_2 \sum_{i,j \in A} \bar{f}_i f_j \left(1 + i \frac{\epsilon^2}{S} \sin \frac{\vec{q} \cdot \vec{r}_{ij}}{2} e^{i\vec{q} \cdot \vec{r}_{ij}/2} \right) e^{-iS\vec{q} \cdot \vec{r}_{ij}} - t_2 \sum_{i,j \in B} \bar{f}_i f_j \left(1 - i \frac{\epsilon^2}{S} \sin \frac{\vec{q} \cdot \vec{r}_{ij}}{2} e^{-i\vec{q} \cdot \vec{r}_{ij}/2} \right) e^{iS\vec{q} \cdot \vec{r}_{ij}} - t_1 \left(\frac{\epsilon}{S} \right)^{2S} \sum_{\substack{i \in A \\ j \in B}} \bar{f}_i f_j \left| \sin \frac{\vec{q} \cdot \vec{r}_{ij}}{2} \right|^{2S} + \text{H.c.}$$

Hopping from
site **A to B**

Hopping from
site **B to A**

$$\begin{aligned}
H = & -t_2 \sum_{i,j \in A} \bar{f}_i f_j \left(1 + i \frac{\epsilon^2}{S} \sin \frac{\vec{q} \cdot \vec{r}_{ij}}{2} e^{i\vec{q} \cdot \vec{r}_{ij}/2} \right) e^{-iS\vec{q} \cdot \vec{r}_{ij}} - t_2 \sum_{i,j \in B} \bar{f}_i f_j \left(1 - i \frac{\epsilon^2}{S} \sin \frac{\vec{q} \cdot \vec{r}_{ij}}{2} e^{-i\vec{q} \cdot \vec{r}_{ij}/2} \right) e^{iS\vec{q} \cdot \vec{r}_{ij}} \\
& - t_1 \left(\frac{\epsilon}{S} \right)^{2S} \sum_{\substack{i \in A \\ j \in B}} \bar{f}_i f_j \left| \sin \frac{\vec{q} \cdot \vec{r}_{ij}}{2} \right|^{2S} + \text{H.c.}
\end{aligned}$$



$$H = \sum_{\vec{k}} \bar{\psi}_{\vec{k}} \mathcal{H}(\vec{k}) \psi_{\vec{k}}.$$



$$\begin{aligned}
\mathcal{H}(\vec{k}) = & \left\{ t_2 \sum_n \cos \vec{k} \cdot \vec{b}_n \left[\cos S\vec{q} \cdot \vec{b}_n - \frac{\epsilon^2}{S} \sin \frac{\vec{q} \cdot \vec{b}_n}{2} \sin \frac{(2S-1)\vec{q} \cdot \vec{b}_n}{2} \right] \right\} \cdot \mathcal{I} + \left\{ t_1 \left(\frac{\epsilon}{S} \right)^{2S} \sum_n \cos \vec{k} \cdot \vec{a}_n \left| \sin \frac{\vec{q} \cdot \vec{a}_n}{2} \right|^{2S} \right\} \cdot \sigma_x \\
& + \left\{ t_1 \left(\frac{\epsilon}{S} \right)^{2S} \sum_n \sin \vec{k} \cdot \vec{a}_n \left| \sin \frac{\vec{q} \cdot \vec{a}_n}{2} \right|^{2S} \right\} \cdot \sigma_y + \left\{ t_2 \sum_n \sin \vec{k} \cdot \vec{b}_n \left[\sin S\vec{q} \cdot \vec{b}_n + \frac{\epsilon^2}{S} \sin \frac{\vec{q} \cdot \vec{b}_n}{2} \cos \frac{(2S-1)\vec{q} \cdot \vec{b}_n}{2} \right] \right\} \cdot \sigma_z.
\end{aligned} \tag{25}$$

$$\begin{aligned}
\mathcal{H}(\vec{k}) = & \left\{ t_2 \sum_n \cos \vec{k} \cdot \vec{b}_n \left[\cos S\vec{q} \cdot \vec{b}_n - \frac{\epsilon^2}{S} \sin \frac{\vec{q} \cdot \vec{b}_n}{2} \sin \frac{(2S-1)\vec{q} \cdot \vec{b}_n}{2} \right] \right\} \cdot \mathcal{I} + \left\{ t_1 \left(\frac{\epsilon}{S} \right)^{2S} \sum_n \cos \vec{k} \cdot \vec{a}_n \left| \sin \frac{\vec{q} \cdot \vec{a}_n}{2} \right|^{2S} \right\} \cdot \sigma_x \\
& + \left\{ t_1 \left(\frac{\epsilon}{S} \right)^{2S} \sum_n \sin \vec{k} \cdot \vec{a}_n \left| \sin \frac{\vec{q} \cdot \vec{a}_n}{2} \right|^{2S} \right\} \cdot \sigma_y + \left\{ t_2 \sum_n \sin \vec{k} \cdot \vec{b}_n \left[\sin S\vec{q} \cdot \vec{b}_n + \frac{\epsilon^2}{S} \sin \frac{\vec{q} \cdot \vec{b}_n}{2} \cos \frac{(2S-1)\vec{q} \cdot \vec{b}_n}{2} \right] \right\} \cdot \sigma_z.
\end{aligned} \tag{25}$$

$H(\vec{k})$ is a 2×2 matrix. In terms of Pauli matrices it is represented as

$$\mathcal{H}(\vec{k}) = \mathcal{H}_0 \mathcal{I} + \mathcal{H}_x(\vec{k}) \sigma_x + \mathcal{H}_y(\vec{k}) \sigma_y + \mathcal{H}_z(\vec{k}) \sigma_z,$$

$$\text{where } \mathcal{H}_0(\vec{k}) = \frac{H_{i,j \in A} + H_{i,j \in B}}{2}, \quad \mathcal{H}_x(\vec{k}) = \text{Re}[H_{i \in A, j \in B}],$$

$$\mathcal{H}_z(\vec{k}) = \frac{H_{i,j \in A} - H_{i,j \in B}}{2}, \quad \mathcal{H}_y(\vec{k}) = \text{Im}[H_{i \in A, j \in B}].$$

Here, \mathcal{I} is the 2×2 unit matrix; σ_x , σ_y , and σ_z are the Pauli matrices.

Lattice vectors

$$\vec{a}_1 = \left(\frac{\sqrt{3}d}{2}, \frac{d}{2} \right), \quad \vec{a}_2 = \left(-\frac{\sqrt{3}d}{2}, \frac{d}{2} \right), \quad \vec{a}_3 = (0, d),$$

$$\vec{b}_1 = \left(-\frac{\sqrt{3}d}{2}, \frac{3d}{2} \right), \quad \vec{b}_2 = \left(-\frac{\sqrt{3}d}{2}, -\frac{3d}{2} \right),$$

$$\vec{b}_3 = (\sqrt{3}d, 0).$$

The chern number at this value is:

$$c_1 = \text{sgn}(\sin Sq), \quad -\frac{\sqrt{3}\pi}{2} \leq q \leq \frac{\sqrt{3}\pi}{2}.$$

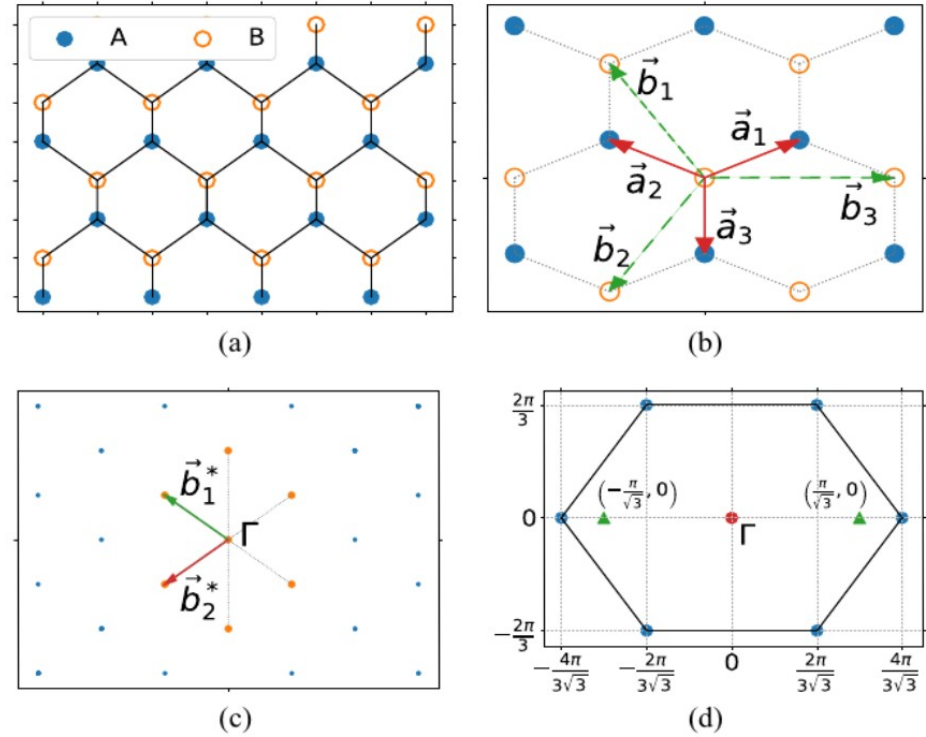
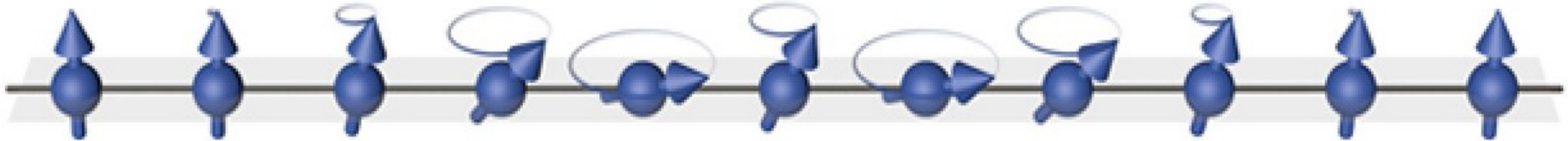


FIG. 1. (a) Schematic of the honeycomb bipartite lattice with two types of atoms A and B. (b) The NN vectors \vec{a}_1 , \vec{a}_2 , and \vec{a}_3 , and the NNN vectors \vec{b}_1 , \vec{b}_2 , and \vec{b}_3 . (c) The reciprocal space of the honeycomb bipartite lattice. The reciprocal unit vectors are $\vec{b}_1^* = 2\pi(-\frac{1}{\sqrt{3}}, \frac{1}{3})$, $\vec{b}_2^* = 2\pi(-\frac{1}{\sqrt{3}}, -\frac{1}{3})$. (d) The first Brillouin zone of the honeycomb bipartite lattice. The special points (triangle), when terms $\sim\sigma_x$ and $\sim\sigma_y$ are zero, for $\vec{q} = (2q/\sqrt{3}, 0)$ lie at $\vec{K} = (\pm\pi/\sqrt{3}, 0)$.

The chern number at this value is:

$$c_1 = \text{sgn}(\sin Sq), \quad -\frac{\sqrt{3}\pi}{2} \leq q \leq \frac{\sqrt{3}\pi}{2}.$$

The chern number depends on the **atomic spin S** and on the **spin wave vector q**



Hall conductivity is : $\rho_{xy} = -\frac{2\pi\hbar}{e^2 c_1},$

change in c_1 results change in direction of spin currents.

Another spin structure

$$\vec{S}_i = S (\sin \vec{q}_1 \vec{r}_i \cos \vec{q}_2 \vec{r}_i, \sin \vec{q}_1 \vec{r}_i \sin \vec{q}_2 \vec{r}_i, \cos \vec{q}_1 \vec{r}_i).$$

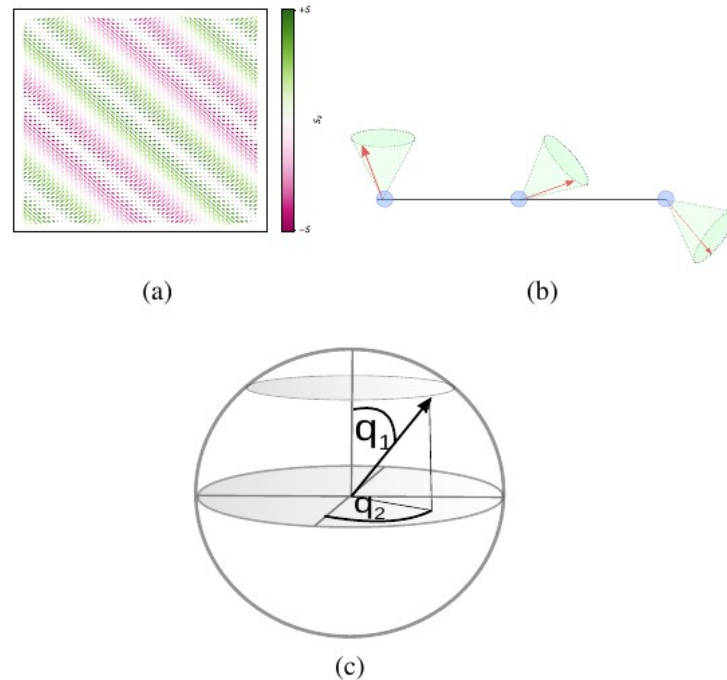


FIG. 1. (a) The spiral spin texture defined by Eq. (1). The direction of the arrows is defined by the S_x and S_y . The color is defined by the S_z components. This spin texture is analogous to the spin texture recently observed in Fe_3GeTe_2 [10]. (b) A 3D representation of the spin configuration on a lattice. The motion of the spin on the surface of the cone is represented by the S_x and S_y components of the Eq. (1); while the Inclination of the cone is represented by the S_z component. (c) Map of the spin texture onto the Bloch sphere.

Another spin structure

$$\vec{S}_i = S (\sin \vec{q}_1 \vec{r}_i \cos \vec{q}_2 \vec{r}_i, \sin \vec{q}_1 \vec{r}_i \sin \vec{q}_2 \vec{r}_i, \cos \vec{q}_1 \vec{r}_i).$$

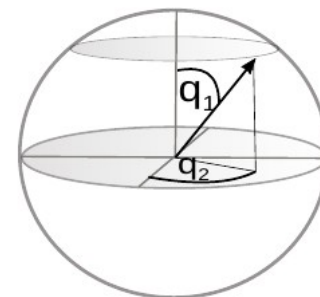
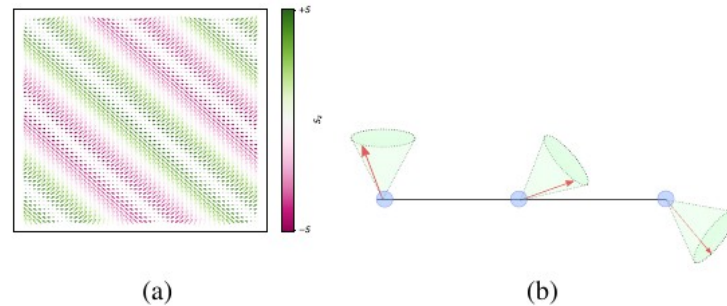


FIG. 1. (a) The spiral spin texture defined by Eq. (1). The direction of the arrows is defined by the S_x and S_y . The color is defined by the S_z components. This spin texture is analogous to the spin texture recently observed in Fe_3GeTe_2 [10]. (b) A 3D representation of the spin configuration on a lattice. The motion of the spin on the surface of the cone is represented by the S_x and S_y components of the Eq. (1); while the Inclination of the cone is represented by the S_z component. (c) Map of the spin texture onto the Bloch sphere.

The chern number for this spin structure:

$$c_1 = \text{sgn} [\sin (S q_{2x})], \quad -\frac{\sqrt{3}\pi}{2} \leq q_{2x} \leq \frac{\sqrt{3}\pi}{2}.$$

Main physical conclusion

- For strongly correlated materials the spin structures have **localized character**.
- No matter how complex is the spin structure the topological properties (Chern number) depends on the **change in spin in neighbouring sites**.
- General expression for Chern number is:

$$c_1 = \text{sgn} \left\{ \sin S \left[\text{atan} \left(\frac{S_{j,y}}{S_{j,x}} \right) - \text{atan} \left(\frac{S_{i,y}}{S_{i,x}} \right) \right] \right\}.$$

Conclusions

- In vdW magnets Chern number depends on the **atomic spin and spin wave vectors**.
- Strong correlation gives rise to the localization of the spin properties, i.e. **no matter how complex is the spin texture, the topological properties depends only on a single factor:** the change in azimuthal angle between neighboring spins.

Publications

- 1) **K. K. Kesharpu**, E. A. Kochetov, and A. Ferraz, **Physical Review B 107, 155146 (2023)**.
- 2) **K. K. Kesharpu**, arXiv:2305.13423, **submitted to PRB (second round review)**